High-Pressure Phases of Calcium: Density-Functional Theory and Diffusion Quantum Monte Carlo Approach

A. M. Teweldeberhan,[1] J. L. Dubois,[1] and S. A. Bonev[1,2,*]

[1]*Lawrence Livermore National Laboratory, P.O. Box 808, Livermore, California 94550, USA*
[2]*Department of Physics, Dalhousie University, Halifax, Nova Scotia, B3H 3J5, Canada*

(Received 6 October 2010; published 3 December 2010)

The phase diagram of Ca is examined using a combination of density-functional theory (DFT) and diffusion quantum Monte Carlo (DMC) calculations. Gibbs free energies of several competing structures are computed at pressures near 50 GPa. Existing disagreements for the stability of Ca both at low and room temperature are resolved with input from DMC. Furthermore, DMC calculations are performed on 0 K crystalline structures up to 150 GPa and it is demonstrated that the widely used generalized gradient approximation of DFT is insufficient to accurately account for the relative stability of the high-pressure phases of Ca. The results indicate that the theoretical phase diagram of Ca needs a revision.

DOI: 10.1103/PhysRevLett.105.235503 PACS numbers: 61.50.Ks, 63.20.D−, 71.15.Pd, 71.15.Mb

Substantial experimental [1–9] and theoretical [10–21] work has been devoted to the study of the electronic, structural, and superconducting properties of Ca at high pressure. Like other alkali and alkaline-earth metals, *s*-to-*d* electron transfer under compression leads to interesting structural transitions. The interest in Ca is also motivated by its remarkable superconducting properties. Starting from about 45 GPa, the superconducting critical temperature (T_c) of Ca increases with pressure and reaches 15 K at 150 GPa [2] and 25 K at 161 GPa [5]. This is the highest observed T_c for a pure element to date. Although knowledge of the structural, dynamical, and electronic properties of Ca at high pressure is essential to explain the superconducting phenomenon, the structure in which it becomes a superconductor is still a subject of debate.

At ambient conditions, Ca crystallizes in the face-centered-cubic (fcc) structure. At higher pressure (P), the following transitions have been observed in x-ray diffraction measurements at room temperature (T): to body-centered-cubic (bcc) at 20 GPa, simple cubic (sc) at 32 GPa, $P4_12_12$ or $P4_32_12$ at 113 GPa, *Cmca* at 139 GPa, and *Pnma* at around 160 GPa [1,3–6,9]. Recently, Mao *et al.* [8] and Nakamoto *et al.* [9] reported that sc Ca undergoes a monoclinic distortion to *Cmmm* upon cooling below 30 K near 45 GPa. Furthermore, Mao *et al.* [8] observed a slight rhombohedral distortion of sc at room T.

Theoretical investigations [10,12,15,17] based on density-functional theory (DFT), on the other hand, found that sc Ca has imaginary phonon frequencies from 0 to 120 GPa, which usually indicates mechanical instability. Furthermore, contrary to experiment, the $I4_1/amd$ structure was reported to have the lowest 0 K enthalpy up to 71 GPa [16,20]. Various other structures, including host-guest [14,20], have been proposed at higher P, but most of them do not match the experimental observations. Errea *et al.* [15] noted that sc must exhibit strong anharmonic effects and Yao *et al.* [16] reported that it has lower room-T enthalpy than $I4_1/amd$ around 40 GPa. However, their result was reversed when the calculations were repeated with a more accurate pseudopotential (PP) [21]. Even approximate inclusion of entropic contributions [21] did not favor sc over $I4_1/amd$ within the generalized gradient approximation (GGA) of DFT.

In this Letter, we first analyze the mechanical and thermodynamic stability of Ca around 50 GPa within GGA-DFT. The analysis includes computing temperature-dependent renormalized phonons and performing thermodynamic integration to obtain Gibbs free energies. Diffusion Monte Carlo (DMC) corrections to the free energies are then included based on a thermodynamic perturbation approach. Finally, DMC calculations are performed on several crystalline structures at 50, 100, and 150 GPa to determine their relative 0 K stability and the results are compared with DFT enthalpies.

We start by examining the dynamical stability of the sc and *Cmmm* structures. Their phonon dispersion relations are first calculated using density-functional perturbation theory as implemented in ABINIT [22]. The calculations were performed with a ten-electron OPIUM PP which includes the $3s$ and $3p$ semicore states as valence states, PBE-GGA [23], a 30-hartree plane-wave cutoff energy and a 16^3 Monkhorst-Pack (MP) mesh for the $\mathbf{k}$-point sampling of the Brillouin zone. The dynamical matrices were computed on 8^3 MP grid. Both structures have imaginary frequencies (see Fig. 1), indicating that in the harmonic approximation and assuming classical particles they should be dynamically unstable (our result for *Cmmm* differs from what was reported in [8,9]).

To go beyond the harmonic approximation, we have carried out Born-Oppenheimer molecular dynamics (MD) simulations using the VASP code [24,25] in a canonical ensemble on sc, $I4_1/amd$, and *Cmmm* supercells consisting of 64 atoms. Convergence was verified with 108- and 125-atom cells for $I4_1/amd$ and sc, respectively.

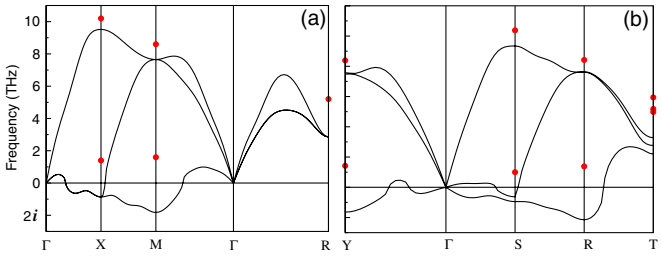

FIG. 1 (color online). Phonon dispersion curves at 45 GPa and 0 K of (a) sc [21] and (b) *Cmmm* from linear response theory. Solid circles are renormalized phonon frequencies from MD at 300 K near 45 GPa.

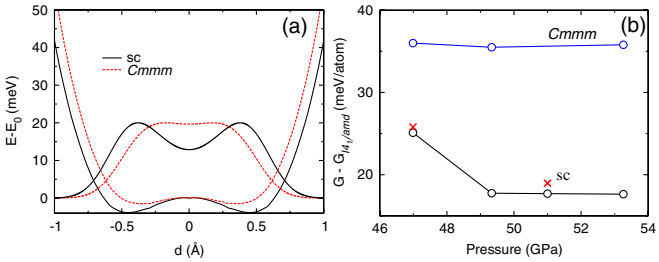

FIG. 2 (color online). (a) Double-well potentials associated with atomic displacements along the transverse soft modes at the M and Y points in sc (solid line) and *Cmmm* (dashed line), respectively. The ground state ionic wave functions for these modes are shown as well. (b) Gibbs free energies from DFT at 300 K of sc and *Cmmm* relative to $I4_1/amd$, with entropy obtained from VDOS (circles) and thermodynamic integration (crosses).

The calculations were performed with a ten-electron PAW PP's, 11-hartree plane-wave cutoff, and the PW91-GGA [26,27] parametrization for the XC functional. The Brillouin zone was sampled at the Γ point for the 108- and 125-atom cells, and 2^3 MP grids were used for the 64-atom cells. The equations of motion were integrated with ionic time steps of 1 fs and the ionic temperature was controlled with a Nosé-Hoover thermostat. Initially, the structures were allowed to equilibrate for 3 ps at 300 K, after which the simulations were continued for an additional 5 ps to gather statistical information. To ensure convergence, selected runs were performed for 7 ps after equilibration. Temperature-dependent renormalized phonon frequencies were then computed at high-symmetry points by Fourier transforming the wave-vector dependent velocity autocorrelation function (VACF). For a given polarization p the autocorrelation function [28] is given by

$$A^p(\mathbf{k}, t) = \frac{\langle v^p_{\mathbf{k}}(t) v^p_{\mathbf{k}}(0)\rangle}{\sum_p \langle v^p_{\mathbf{k}}(0) v^p_{\mathbf{k}}(0)\rangle}, \quad (1)$$

where $v^p_{\mathbf{k}}(t) = \sum_j v^p_j(t) \exp[-i\mathbf{k}\cdot\mathbf{r}_j(t)]$ is the reciprocal space representation of the velocity, $\mathbf{r}_j$ is the position of atom j, v^p_j is the p component of the velocity of atom j, and $\mathbf{k}$ is the wave vector of interest. Phonon frequencies are obtained from the locations of the sharp peaks of the Fourier transformed $A^p(\mathbf{k}, t)$. The results for the sc and *Cmmm* phases at around 45 GPa and 300 K are compared with the 0 K dispersion curves in Fig. 1. Both structures are dynamically stable at finite T and the differences between the MD and harmonic frequencies indicate strong T dependence of the vibrational modes.

The electronic band structures of sc and *Cmmm* have a degeneracy at the Γ point, which is lifted by a Peierls distortion, leading to a small energy gain. Because of symmetry, the potential associated with this distortion has a double-well character, first noted in [15]. As illustrated in Fig. 2(a) with the transverse soft modes of sc and *Cmmm*, the potential barrier of the double well is only a few meV. This means, first, that the entire double-well potential is sampled by the ions at $T \sim 10^2$ K, consistent with our renormalized phonon analysis. Second, the tunneling frequency between the two sides of the well is relatively large even in a quantum mechanical near-ground state. It is 168 GHz in sc and 300 GHz in *Cmmm* with their respective splitting between the lowest symmetric-antisymmetric ionic eigenstates of 0.7 and 1.25 meV; for example, compare this with 24 GHz and 0.1 meV in ammonia. Therefore, even low-T x-ray diffraction experiments will measure atomic positions at the equilibrium sc and *Cmmm* sites, albeit they would exhibit enhanced thermal diffuse scattering.

In order to investigate the thermodynamic stability of the sc phase at finite T, we compare its Gibbs free energy with that of the previously proposed $I4_1/amd$ and *Cmmm* structures. The Gibbs free energy, $G = \langle U\rangle + \langle P\rangle V - \langle T\rangle S$, where $\langle\,\rangle$ represents ensemble (time) average, is computed under fixed number of atoms N, volume V and T, from MD simulations as follows: $\langle U\rangle = \langle E\rangle + \langle E_{\text{kin}}\rangle$ is the sum of the Kohn-Sham energy and the kinetic energy of the ions, $P = -dE/dV + Nk_BT/V$ and the entropy S is obtained initially by integrating the vibrational density of states (VDOS), which is the Fourier transform of the VACF. The relative stability of the aforementioned structures is determined by calculating G as a function of P along isotherms for several densities. Figure 2(b) shows the Gibbs free energies of the sc and *Cmmm* structures relative to $I4_1/amd$ at 300 K. According to these calculations, sc is not preferred at room T up to 80 GPa. We have also computed G of sc and $I4_1/amd$ at 600 and 1000 K between 46 and 54 GPa. The energy difference between the two structures decreases with T favoring the sc structure at 1000 K.

While the VDOS represent temperature-dependent renormalized frequencies, a harmonic partition function is assumed when integrating them to obtain S. This approach does not fully account for anharmonic effects. To fully account for them, we compute corrections to the free energies obtained from VDOS using thermodynamic integration. In this method, MD simulations were carried out

for a system with a potential energy function of the form: $U(\lambda) = U_0 + \lambda(U_1 - U_0)$, where U_0 is the potential energy of a reference system with known free energy and U_1 is the potential energy of the system under investigation. Here λ is a coupling parameter which ranges from zero to unity. The Helmholtz free energy difference between the two systems is given by

$$\Delta F = \int_0^1 d\lambda \left\langle \frac{\partial U(\lambda)}{\partial \lambda} \right\rangle_{N,V,T,\lambda}. \quad (2)$$

The value of the above integral is calculated numerically by performing MD simulations in a canonical ensemble with λ from 0 to 1 in intervals of 0.1. For a reference system, we have chosen an Einstein crystal with a harmonic spring constant fitted to reproduce the Helmholtz free energy obtained earlier from the VDOS integration. With this choice, Eq. (2) represents the full anharmonic correction to the TS term computed from VDOS.

We have performed thermodynamic integration on the sc and $I4_1/amd$ at 300 K for two densities, corresponding to pressures near 47 and 51 GPa. At 47 GPa, ΔF is 6.82 and 6.12 meV for sc and $I4_1/amd$, respectively, confirming that the free energies from VDOS capture most of the anharmonicity: $\Delta F/(TS) = 6\%$. Furthermore, the *relative* free energies of the different structures, shown in Fig. 2(b), are identical within 1 meV between the two methods. Based on these results, we conclude that the apparent thermodynamic stability of sc Ca cannot be established within the framework of the GGA-DFT.

The transition from the highly coordinated fcc and bcc to lower coordinated structures such as sc, $I4_1/amd$, $Pnma$, etc., is driven by s-to-d charge transfer. The difficulties of local density approximations in describing transition metals are well known [29]. Furthermore, we notice the pronounced peak in the electron DOS of $I4_1/amd$, indicating enhanced electron localization [see inset in Fig. 3(a)]. This has prompted us to consider the possibility that there are significant errors originating from the GGA, in particular, in relation to the relative stability of $I4_1/amd$. We have addressed this issue by computing corrections to the DFT free energies with DMC at the level of thermodynamic perturbation, namely: $F_{\mathrm{DMC}} \approx F_{\mathrm{DFT}} + \langle U_{\mathrm{DMC}} - U_{\mathrm{DFT}} \rangle_{\mathrm{DFT}}$.

The fixed node diffusion Monte Carlo (DMC) method samples the *exact* lowest energy eigenvalue of the full many body electronic Hamiltonian given a constraint on the $3N - 1$ dimensional nodal hypersurface [30]. For our DMC calculations, we have used the CASINO package [31] with a Slater-Jastrow guiding function. The nodal constraints were obtained from plane-wave DFT calculations with a hard semicore Troullier-Martins PP with 10 valence electrons and a plane-wave energy cutoff of 35 hartree using the quantum-espresso package [32]. We used a Jastrow term with explicit electron-electron, electron-nucleus, and electron-electron-nucleus correlation functions [33] and optimized the guiding function for each

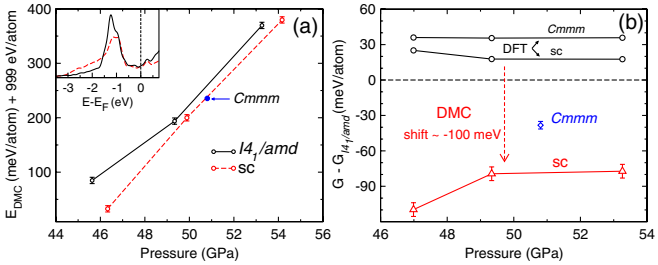

FIG. 3 (color online). (a) DMC energies for sc, $I4_1/amd$, and $Cmmm$ configurations from MD at 300 K. Here 999 eV/atom is an arbitrary reference energy. The inset shows the DFT electronic density of states of sc and $I4_1/amd$ structures at 50 GPa. (b) DMC-corrected Gibbs free energies at 300 K of sc and $Cmmm$ relative to $I4_1/amd$ showing that the sc structure is preferred. DFT results are shown for comparison.

structure within variational Monte Carlo (VMC) method by minimizing the maximum absolute deviation of the VMC energy. Finite-T DMC energies were obtained at three different pressures by solving for the electronic ground state energies of three snapshot structures for each P drawn from the DFT-MD simulations at the (1/4, 1/4, 1/4) **k** point. As a check of **k**-point convergence we also evaluated relative energies between structures obtained from twist averaging [34] over a 2^3 **k**-point grid with no qualitative change in results.

According to our DMC calculations, the sc structure is preferred at 300 K, in agreement with the experimental measurements. Figure 3(a) shows the energies of finite-T configurations of sc, $I4_1/amd$, and $Cmmm$ obtained from DMC. The DMC-corrected Gibbs free energies of the sc and $Cmmm$ structures relative to $I4_1/amd$ are shown in Fig. 3(b). Although the DMC internal energies of sc and $Cmmm$ are almost degenerate at 300 K, the PV and TS terms favor sc. Contrary to the DFT results, both the internal energy and Gibbs free energies of sc are lower than that of $I4_1/amd$. Indeed, the relative energy shift coming from the DMC correction, about 100 meV at 50 GPa, is quite significant and beyond the uncertainties of our calculations. Finally, we note that the slight rhombohedral distortion of sc observed by Mao *et al.* [8] leads to energy change of less than a meV.

The relative 0 K enthalpies at 50, 100, and 150 GPa of recently reported candidate structures computed with DFT and DMC are given in Table I. The DMC energies for 0 K structures were obtained from 32-atom supercells with coordinates relaxed in DFT at fixed pressure, using twist averaging over a $2 \times 2 \times 4$ MP **k**-point mesh. For the enthalpies, DFT pressures were used. The DMC calculations reveal that the $Cmmm$ structure is preferred at low T at 50 and 100 GPa. This is in agreement with the recent experimental work of Mao *et al.* [8] and Nakamoto *et al.* [9]. It is worth mentioning that $I4_1/amd$ [16,20] and the incommensurate $I4/mcm(00\gamma)$ structure [14] are not preferred within DMC. Note that we cannot make a direct

TABLE I. DFT-GGA and DMC enthalpies. For each P, ΔH is the 0 K enthalpy difference with respect to the lowest enthalpy structure.

DFT P (GPa)	DFT		DMC	
	Phase	ΔH (meV)	Phase	ΔH (meV)
	$I4_1/amd$	0	$Cmmm$	0
50	$Pnma$	28.6	sc	61(2)
	sc	50.3	$I4_1/amd$	82(3)
	$Cmmm$	50.4	$Pnma$	96(2)
	$P4_32_12$	0	$Cmmm$	0
	$Cmca$	14.2	sc	14(4)
100	$Pnma$	18.1	$P4_32_12$	68(3)
	$I4_1/amd$	61.4	$Cmca$	88(3)
	$Cmmm$	95.0	$Pnma$	153(6)
	sc	102.6	$I4_1/amd$	157(7)
	$I4/mcm(00\gamma)$	0	$Pnma$	0
150	$Pnma$	11.6	$I4/mcm(00\gamma)$	51(3)
	$Cmca$	49.4	$P4_32_12$	81(4)
	$P4_32_12$	71.2	$Cmca$	98(7)

comparison with available x-ray measurements above 100 GPa. First, these experiments were conducted at room T and second, we are using the DFT pressure. A rough finite-difference estimate of P for several structures near 100 GPa shows that the DMC pressure is systematically higher by about 10 GPa. The important result here is the comparison between the two theoretical methods, showing that GGA-DFT does not predict accurately the lowest energy structures. Other properties of Ca, e.g., superconductivity, computed within DFT may also have inaccuracies and need a revision.

In summary, we have investigated the stability of the high-pressure phases of Ca. Errors that arise from the exchange-correlation functional approximation of DFT have been corrected with DMC to resolve discrepancies between DFT calculations and experiment. A detailed analysis of the high-pressure structures of Ca with more accurate methods such as DMC is required to construct its entire phase diagram and electronic properties. Our findings for Ca may have relevance for other materials exhibiting s-to-d transitions under pressure.

Work at LLNL prepared under Co. DE-AC52-07NA27344. A. M. T. and S. A. B. acknowledge support from NSERC, ACEnet, and CFI.

*bonev@llnl.gov

[1] H. Olijnyk and W. B. Holzapfel, Phys. Lett. A **100**, 191 (1984).
[2] S. Okada, K. Shimizu, T. Kobayashi, K. Amaya, and S. Endo, J. Phys. Soc. Jpn. **65**, 1924 (1996).
[3] D. Errandonea, R. Boehler, and M. Ross, Phys. Rev. B **65**, 012108 (2001).
[4] T. Yabuuchi, Y. Nakamoto, K. Shimizu, and T. Kikegawa, J. Phys. Soc. Jpn. **74**, 2391 (2005).
[5] T. Yabuuchi, T. Matsuoka, Y. Nakamoto, and K. Shimizu, J. Phys. Soc. Jpn. **75**, 083703 (2006).
[6] H. Fujihisa, Y. Nakamoto, K. Shimizu, T. Yabuuchi, and Y. Gotoh, Phys. Rev. Lett. **101**, 095503 (2008).
[7] Q. F. Gu, G. Krauss, Yu. Grin, and W. Steurer, Phys. Rev. B **79**, 134121 (2009).
[8] W. L. Mao *et al.*, Proc. Natl. Acad. Sci. U.S.A. **107**, 9965 (2010).
[9] Y. Nakamoto *et al.*, Phys. Rev. B **81**, 140106(R) (2010).
[10] G. Gao, Y. Xie, T. Cui, Y. Ma, L. Zhang, and G. Zou, Solid State Commun. **146**, 181 (2008).
[11] Y. Yao, J. S. Tse, Z. Song, D. D. Klug, J. Sun, and Y. Le Page, Phys. Rev. B **78**, 054506 (2008).
[12] A. M. Teweldeberhan and S. A. Bonev, Phys. Rev. B **78**, 140101(R) (2008).
[13] T. Ishikawa, A. Ichikawa, H. Nagara, M. Geshi, K. Kusakabe, and N. Suzuki, Phys. Rev. B **77**, 020101(R) (2008).
[14] S. Arapan, H. Mao, and R. Ahuja, Proc. Natl. Acad. Sci. U.S.A. **105**, 20627 (2008).
[15] I. Errea, M. Martinez-Canales, A. R. Oganov, and A. Bergara, High Press. Res. **28**, 443 (2008).
[16] Y. Yao, D. D. Klug, J. Sun, and R. Martonak, Phys. Rev. Lett. **103**, 055503 (2009).
[17] Z. P. Yin, F. Gygi, and W. E. Pickett, Phys. Rev. B **80**, 184515 (2009).
[18] S. L. Qiu and P. M. Marcus, J. Phys. Condens. Matter **21**, 435403 (2009).
[19] T. Ishikawa, H. Nagara, N. Suzuki, T. Tsuchiya, and J. Tsuchiya, Phys. Rev. B **81**, 092104 (2010).
[20] A. R. Oganov, Y. Ma, Y. Xu, I. Errea, A. Bergara, A. O. Lyakhov, Proc. Natl. Acad. Sci. U.S.A. **107**, 7646 (2010).
[21] A. M. Teweldeberhan and S. A. Bonev, Phys. Rev. Lett. **104**, 209601 (2010).
[22] X. Gonze *et al.*, Comput. Mater. Sci. **25**, 478 (2002).
[23] J. P. Perdew, K. Burke, and M. Ernzerhof, Phys. Rev. Lett. **77**, 3865 (1996).
[24] G. Kresse and J. Hafner, Phys. Rev. B **47**, 558 (1993).
[25] G. Kresse and J. Furthmüller, Phys. Rev. B **54**, 11 169 (1996).
[26] Y. Wang and J. P. Perdew, Phys. Rev. B **44**, 13 298 (1991).
[27] J. P. Perdew *et al.*, Phys. Rev. B **46**, 6671 (1992).
[28] N. I. Papanicolaou, I. E. Lagaris, and G. A. Evangelakis, Surf. Sci. **337**, L819 (1995).
[29] R. E. Watson, G. W. Fernando, M. Weinert, Y. J. Wang, and J. W. Davenport, Phys. Rev. B **43**, 1455 (1991).
[30] See, e.g., W. M. C. Foulkes, L. Mitas, R. J. Needs, and G. Rajagopal, Rev. Mod. Phys. **73**, 33 (2001).
[31] R. J. Needs, M. D. Towler, N. D. Drummond, and P. Lpez Ros, J. Phys. Condens. Matter **22**, 023201 (2010).
[32] P. Giannozzi *et al.*, http://www.quantum-espresso.org.
[33] N. D. Drummond, M. D. Towler, and R. J. Needs, Phys. Rev. B **70**, 235119 (2004).
[34] C. Lin, F. H. Zong, and D. M. Ceperley, Phys. Rev. E **64**, 016702 (2001).